SIDEBAR 5.2: RADIATIVE FORCING BY BLACK CARBON IN THE ARCTIC—P. K. QUINN, A. STOHL, A. BAKLANOV, M. G. FLANNER, A. HERBER, K. KUPIAINEN, K. S. LAW, J. SCHMALE, S. SHARMA, V. VESTRENG, AND K. VON SALZEN

Black carbon (BC) is the most efficient atmospheric particulate species at absorbing visible light. Consequently, it exerts a warming effect that contrasts with the cooling effect of purely scattering aerosol components such as sulfate. However, pure BC particles rarely occur in the atmosphere. Soon after emission, BC becomes mixed with other components such as sulfate and organics. BC-containing particles can have either a warming or a cooling effect on climate depending on their altitude and the albedo of the underlying surface relative to the albedo of the BC haze itself. The albedo of the haze depends on the relative amounts of all of the chemical components present, their mixing state, and whether they primarily scatter or absorb light. BC-containing aerosols, unlike greenhouse gases, are short-lived, with a lifetime in the atmosphere on the order of days to weeks. While recognizing that reductions in CO_2 emissions are required for long-term mitigation of Arctic warming, it has been suggested that reducing emissions of BC could reduce projected global mean warming and slow the rate of warming in the short term in the Arctic (Shindell et al. 2012; Bowerman et al. 2013).

Atmospheric BC concentrations in the Arctic have declined since the 1990s (Sharma et al. 2013), and the BC content of Arctic snow is now no higher than it was thirty years ago (Clarke and Noone 1985; Doherty et al. 2010), but BC-containing aerosols will likely continue to influence Arctic climate through several different forcing mechanisms. Atmospheric BC can directly warm the Arctic atmosphere by absorbing solar radiation that would otherwise have been reflected back to space or absorbed by the surface (far right panel in Fig. SB5.4). The added atmospheric heating subsequently increases the downward longwave radiation to the surface and decreases the temperature difference between the surface and the atmosphere, thereby warming the surface. With the highly reflective snow and ice surfaces typical of the Arctic, even a moderately absorbing aerosol can lead to a heating of the surface–atmosphere column. The average daily radiative efficiency of atmospheric BC (units of W g^{-1}) in the Arctic summer is greater than in most other environments because of the long sunlight exposure and presence of highly reflective clouds, snow, and sea ice (e.g., Cess 1983). As summer progresses and open water appears within the sea ice cover, and melt ponds form on the ice surface, the direct forcing efficiency by atmospheric BC decreases because the surface becomes less reflective. Similarly, it is reasonable to expect that forcing by atmospheric BC will become weaker as snow, sea ice, and glacier extent and surface albedo decrease under a warming climate (Flanner et al. 2009).

BC deposited to snow and ice surfaces enhances the absorption of solar radiation at the surface and warms the lower atmosphere, which can initiate snow and ice melt earlier in the season (left center panel in Fig. SB5.4). Even very low BC concentrations (ppb) of deposited BC have an impact because the absorptivity of BC is about five orders of magnitude greater than ice at visible wavelengths. In addition, multiple scattering in surface snow greatly increases the path-length of photons and the probability that they will encounter non-ice particles (Warren and Wiscombe 1980). Snow darkening drives an equilibrium temperature response, per unit of radiative forcing, several times that of CO_2 (Koch et al. 2009). This large impact occurs because all of the energy associated with the forcing is deposited directly into the snow and ice covers, components of the Earth system responsible for powerful positive feedback (e.g, Robock 1983; Hansen and Nazarenko 2004).

Radiative forcing by BC can also result from the impact of aerosols on cloud distributions, lifetime, and microphysical properties. By increasing the number of cloud droplets and decreasing cloud droplet size, aerosols can lead to an increase in reflectivity and cloud optical thickness (first indirect effect) and to an increase in cloud lifetime and a decrease in precipitation (second indirect effect; e.g., Twomey 1977). Both of these changes result in greater reflection of solar shortwave radiation back to space and a cooling at the surface (right center panel in Fig. SB5.4). In contrast, when the cloud droplet number concentration of thin Arctic liquid-phase clouds is increased through interaction with anthropogenic aerosols, the clouds become more efficient at trapping and re-emitting longwave radiation, which results in a warming at the surface (Garrett and Zhao 2006; far left column in Fig. SB5.4). BC can also impact clouds through semi-direct effects associated with atmospheric heating. Depending on circumstances, BC-induced heating can either stabilize the atmosphere and increase low-level cloud formation (Hansen et al. 2005), inhibit cloud formation, or increase

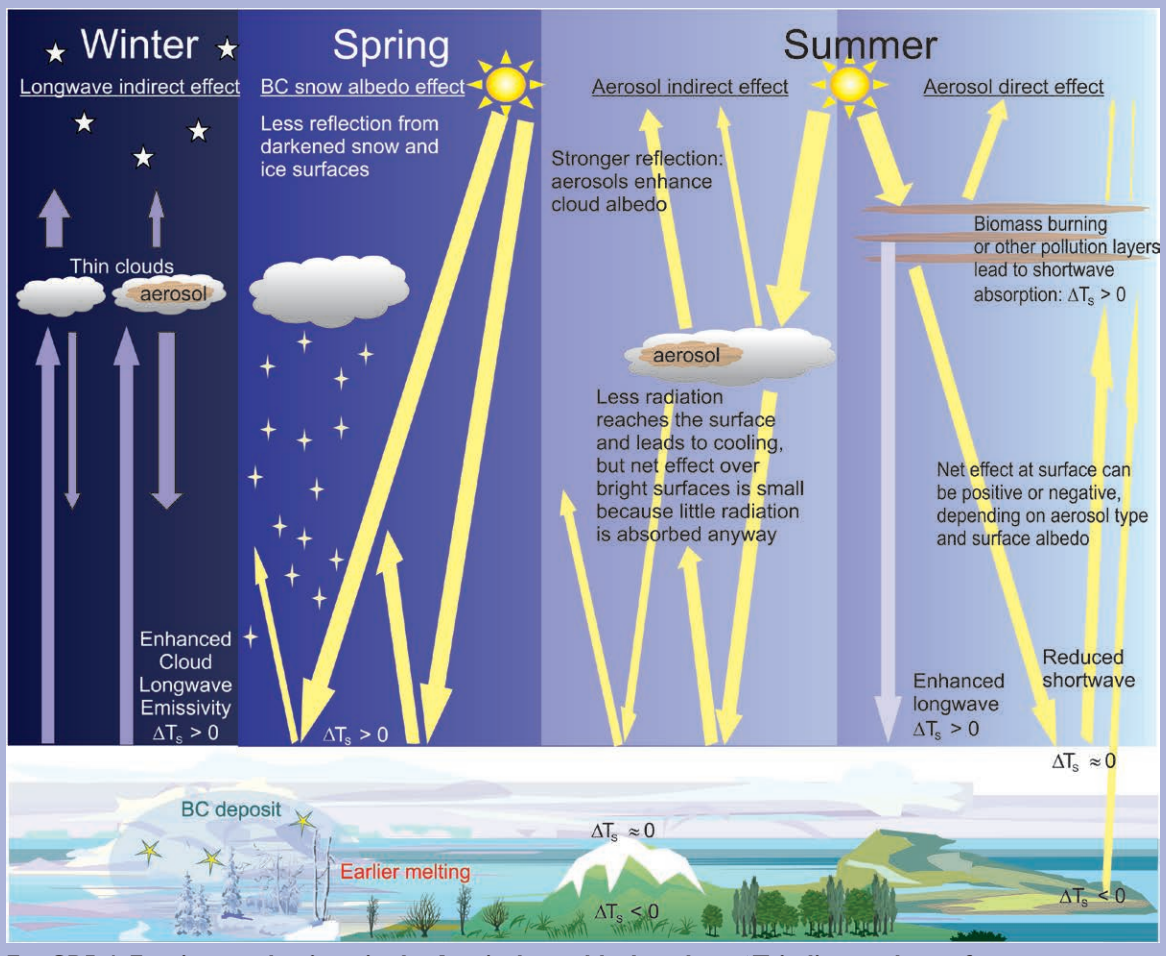

Fig. SB5.4. Forcing mechanisms in the Arctic due to black carbon. ΔT_s indicates the surface temperature response.

the evaporation rate of clouds (e.g., Ackerman et al. 2000; Jacobson 2010). Simulating these indirect and semi-direct effects remains a challenge for global-scale models, especially in the Arctic. Both the sign and magnitude of the net forcing due to nonlinear interactions between BC and clouds in the Arctic are uncertain.

Further complicating the impact of BC on Arctic climate is that forcing exerted by BC outside of the Arctic can result in changes in energy transport through the atmosphere and oceans to the Arctic (Shindell and Faluvegi 2009). For example, BC-heated air masses can travel from midlatitudes to the Arctic.

In the past few years there has been a concerted effort by the scientific community to quantitatively estimate the climate impacts of BC, both globally and within the Arctic (e.g., Bond et al. 2013; Quinn et al. 2008). Currently, there is no single appropriate environmental indicator to assess the Arctic climate response to changes in emissions of BC and co-emitted species including organic carbon and sulfate. Hence, only an integrated evaluation will reduce the large uncertainties and improve estimates of BC's climate impacts. Such an evaluation requires accurate emission inventories of local and remote sources, long-term monitoring and process-oriented measurements, and global models capable of realistic transport of BC to the Arctic and depositional losses en route and within the Arctic. In addition, models must accurately capture feedbacks induced by BC, including those associated with snow, glacier, and sea-ice loss, cloud changes, and dynamical changes.

Measurements made by both approaches are typically calibrated with standards based on WMO mole fraction scales maintained at NOAA ESRL. Uncertainties estimated using a Monte Carlo method for the NOAA zonal means in Figs. 5.11a and 5.11b are 0.3–0.6 ppm for CO_2 and 2–4 ppb for CH_4 weekly averages.

Observations of atmospheric CO_2 (Fig. 5.11a) averaged for the Arctic observation sites show that CO_2 continued to increase in 2013 (3.2 ppm higher than in 2012, the same as the global increase). At present, trends in Arctic atmospheric CO_2 due to changes in Arctic productivity or respiration are difficult to distinguish from midlatitude anthropogenic emissions; most of the increase in atmospheric CO_2 in the Arctic is from combustion of fossil fuels at midlatitudes.

After a period of stability from 1999 to 2006 (the reasons for this are not fully understood and it is a topic of continuing research), CH_4 in the Arctic atmosphere began increasing in 2007 (Fig. 5.11b). In 2013, CH_4 was 5.0 ppb (preliminary estimate) higher than in 2012, equal to the increase in global CH_4. The increase in global CH_4 is attributed to a combination of increased tropical natural emissions and emissions from fossil fuel production, agriculture, and waste (Bruhwiler et al. 2014; Bergamaschi et al. 2013). Although interannual variability in Arctic emissions is captured in the Arctic observations, large sustained increases in CH_4 emissions from Arctic sources have not been observed.

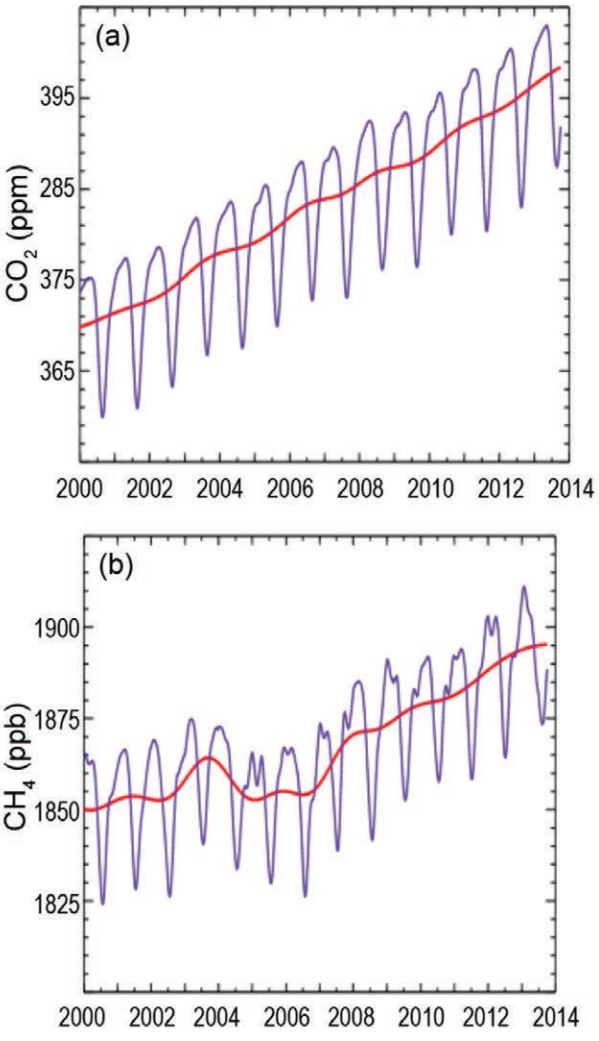

Fig. 5.11. Weekly averages of (a) CO_2 (ppm) and (b) CH_4 (ppb) for 16 high northern latitude sites (blue curves) with deseasonalized trends (red curves). The seasonal CO_2 cycle reflects uptake by the terrestrial biosphere during the NH growing season and respiration during the winter months. The minimum in the CH_4 seasonal cycle occurs during the NH summer due to solar radiation-dependent photochemical destruction.

f. Sea ice cover—D. Perovich, S. Gerland, S. Hendricks, W. Meier, M. Nicolaus, J. Richter-Menge, and M. Tschudi

1) Sea ice extent

Sea ice extent is a fundamental descriptor of the state of the Arctic sea ice cover. Satellite-based passive microwave instruments have been used to determine sea ice extent since 1979. There are two months each year that are of particular interest: September, at the end of summer, when the sea ice reaches its annual minimum extent, and March, at the end of winter, when the ice reaches its annual maximum extent. The sea ice extent in March 2013 and September 2013 are presented in Fig. 5.12.

Based on estimates produced by the National Snow and Ice Data Center (NSIDC), the sea ice cover reached a minimum annual extent of 5.10 million

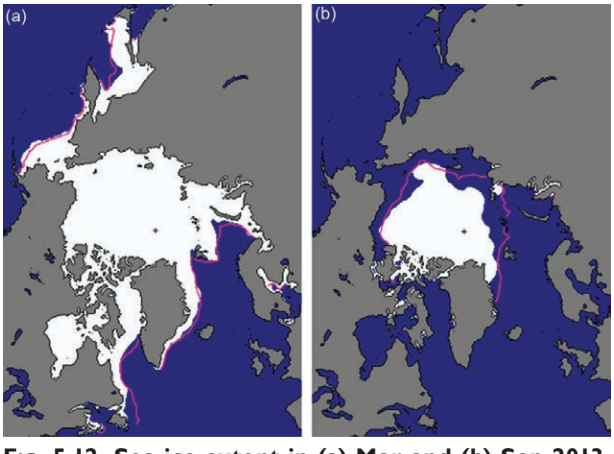

Fig. 5.12. Sea ice extent in (a) Mar and (b) Sep 2013, illustrating the respective monthly averages during the winter maximum and summer minimum extents. The magenta lines indicate the median ice extents during the period 1981–2010. (Source: NSIDC, http://nsidc.org/data/seaice_index.)

km² on 13 September 2013. This was 1.69 million km² higher than the record minimum of 3.41 million km² set in 2012 and the largest September minimum ice extent since 2006 (Fig. 5.13). However, the 2013 summer minimum extent was still 1.12 million km² (18%) below the 1981–2010 average minimum ice extent. The March 2013 ice extent reached a maximum value of 15.04 million km² (Fig. 5.13), 3% below the 1981–2010 average. This was slightly less than the March 2012 value, but typical of the past decade.

The September monthly average trend is –13.7% decade^{-1} relative to the 1981–2010 average (Fig. 5.13). Trends are smaller during March (–2.4% decade^{-1}) but are still decreasing and statistically significant. There was a loss of 9.69 million km² of sea ice between the March and September extents. This is the smallest seasonal decline since 2006.

2) Age of the ice

Key ice physical properties, such as surface roughness, melt pond coverage, and thickness, vary according to the age of the ice. The age of the ice can be determined using satellite observations and drifting buoy records to track ice parcels over several years (Tschudi et al. 2010). This method has been used to provide a record of ice age since 1984. The distribution of ice of different ages (Fig. 5.14) illustrates the extensive loss in recent years of the older ice types (Maslanik et al. 2011).

Although the minimum sea ice extent increased somewhat in 2013 compared to recent years, the distribution of ice age continued to favor first-year ice (ice that has not survived a melt season), which is the thinnest ice type (e.g., Maslanik et al. 2007). In March 1988, 58% of the ice pack was composed of first-year ice, an amount that increased to 78% in March 2013. Meanwhile, the trends continue for the recent loss of the oldest and thicker ice types, which accelerated starting in 2005 (Maslanik et al. 2011). For the month of March, the oldest ice (four years and older) decreased from 26% of the ice cover in 1988 to 19% in 2005 and to 7% in 2013.

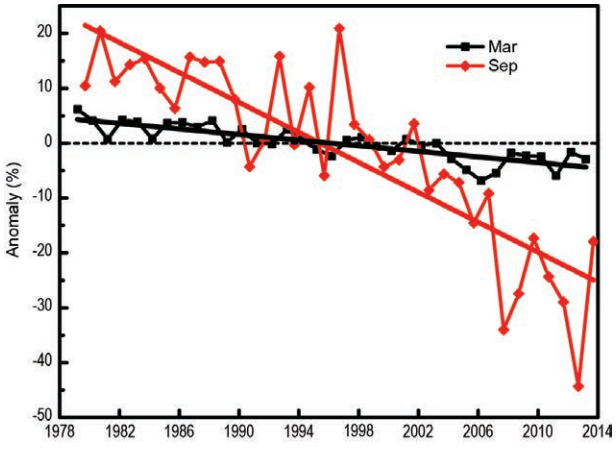

Fig. 5.13. Time series of ice extent anomalies measured in Mar (maximum ice extent) and Sep (minimum ice extent). The anomaly value for each year is the difference (in %) in ice extent relative to the average values for the period 1981–2010. The black and red lines are least squares linear regression lines.

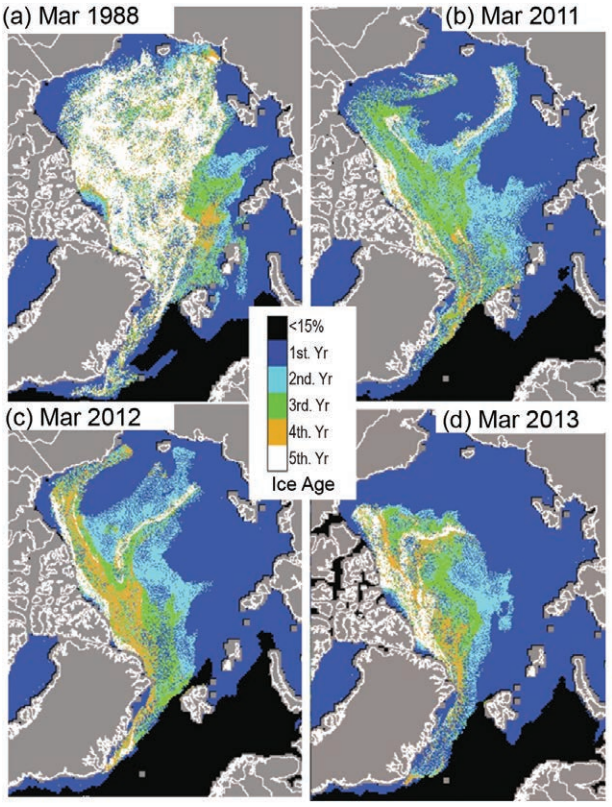

Fig. 5.14. Sea ice age in Mar (a) 1988, (b) 2011, (c) 2012, and (d) 2013, determined using satellite observations and drifting buoy records to track the movement of ice floes.

At the end of winter 2012/13, little multiyear ice was detected in much of the Beaufort Sea (Fig. 5.14d; Richter-Menge and Farrell 2013). There is no precedent in the satellite-derived record of ice age for the near-absence of old ice in this region. This condition appears to have been due to a combination of the previous year's record sea ice retreat and a lack of subsequent transport of multiyear ice into the Beaufort Sea during winter 2012/13. Negligible multiyear ice transport into the Beaufort Sea continued during summer 2013, consistent with stronger cyclonic (counterclockwise) wind forcing during this period (see section 5g). Multiyear ice did not drift into Siberian Arctic waters either, which is also rare. Instead,

multiyear ice remained confined to the region north of Greenland and northernmost Canada during 2013.

3) Ice thickness

Another key state variable for the Arctic sea ice cover is ice thickness. In recent years, ice thickness has been estimated over limited regions by aircraft, e.g., the NASA Operation IceBridge (Richter-Menge and Farrell 2013), and over large regions by satellite. The CryoSat-2 satellite, operated since 2011 by the European Space Agency, measures ice freeboard, the height of ice floes above the water line. Preliminary analysis indicates that the CryoSat-2 freeboard estimates are comparable to in situ field measurements, with a level of uncertainty that is comparable to other airborne and satellite-based observations (Ricker et al. 2014). Calculation of the actual sea-ice thickness from freeboard requires knowledge of snow depth, but in general higher freeboard indicates thicker sea ice. Therefore, freeboard maps in spring for the period 2011–13 are a proxy for sea ice thickness at the time of maximum ice extent. During the three years of CryoSat-2 observations, the average freeboard within the Arctic Basin decreased by 0.04 m, from 0.23 m in 2011 to 0.19 m in 2013 (Laxon et al. 2013). Assuming there were no significant changes in snow depth, the decline in freeboard amounts to an average sea ice thinning of 0.32 m, from 2.26 m in 2011 to 1.94 m in 2013. As with the ice age maps (Fig. 5.14), CryoSat-2 freeboard maps (Perovich et al. 2013, figure 22) indicate that most of the thickest and oldest ice occurs to the north of Greenland and northernmost Canada, and is a small proportion of the total sea ice cover at the end of winter.

g. Ocean temperature and salinity—M.-L. Timmermans, I. Ashik, I. Frolov, H. K. Ha, R. Ingvaldsen, T. Kikuchi, T. W. Kim, R. Krishfield, H. Loeng, S. Nishino, R. Pickart, I. Polyakov, B. Rabe, U. Schauer, P. Schlosser, W. M. Smethie, V. Sokolov, M. Steele, J. Toole, W. Williams, R. Woodgate, and S. Zimmerman

1) Summer sea surface temperature

Recent summers with reduced sea-ice cover (see section 5f) have seen increased solar absorption into the surface Arctic Ocean, with the distribution of sea surface temperatures (SST) reflecting sea ice retreat patterns. Arctic Ocean average SSTs in August 2013 ranged between ~0° and 4°C, with even higher SSTs in some marginal seas (Fig. 5.15). While most Arctic boundary regions displayed anomalously warm SSTs in August 2013, relative to the 1982–2006 August average (Fig. 5.15), cold anomalies were evident in the Chukchi and East Siberian Seas. The cooler SSTs

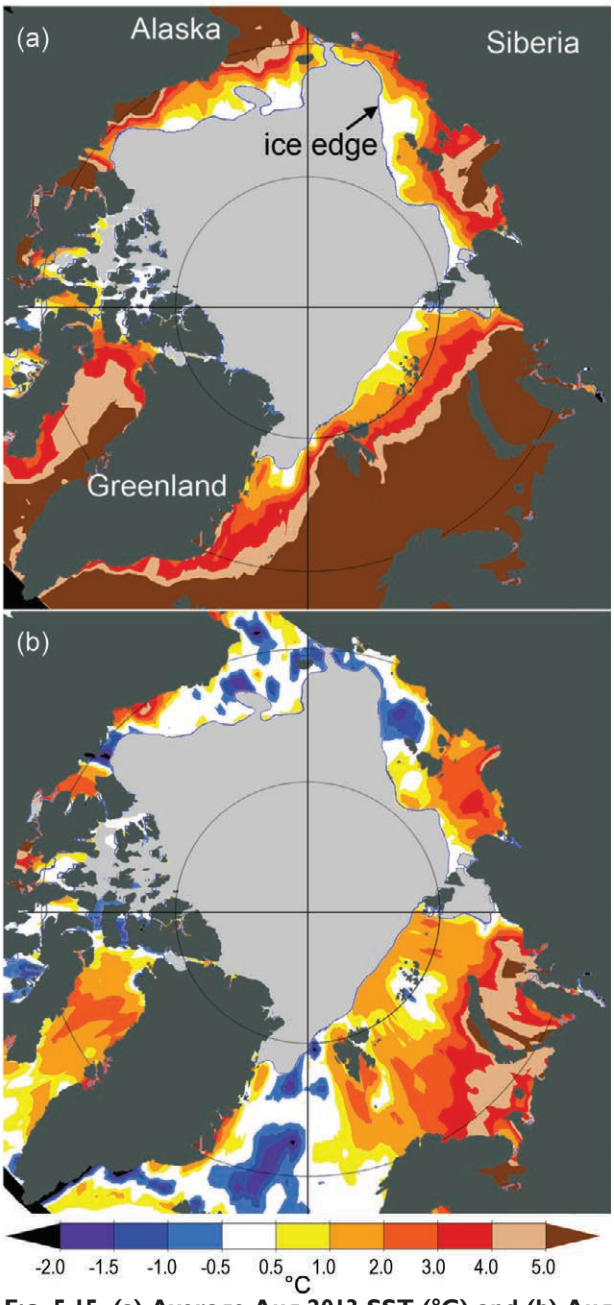

Fig. 5.15. (a) Average Aug 2013 SST (°C) and (b) Aug 2013 SST anomalies (°C) relative to the Aug 1982–2006 average. Anomalies are derived from satellite data according to Reynolds et al. (2007). The gray area shows the average Aug 2013 sea-ice extent according to the National Snow and Ice Data Center.

in these regions are linked to later and less extensive sea-ice retreat; anomalously cold August SSTs related to unusual sea-ice extent patterns were also observed in this region in 2012 (Timmermans et al. 2013b). Anomalously warm August SSTs in the Barents and Kara Seas are related to earlier ice retreat in these regions and possibly also to the advection of anomalously warm water from the North Atlantic.

Hydrographic data show surface waters in the vicinity of the Barents Sea Opening in September 2013 were about 3°C warmer than in September 2012. SSTs in the southern Barents Sea in September 2013 were as high as 11°C and up to 5°C above the 1977–2006 average (Trofimov and Ingvaldsen 2014).

2) Upper ocean salinity

Salinity in the upper several hundred meters of the Arctic Ocean is set by sea ice melt/growth cycles, influxes from the Pacific and Atlantic oceans, river input, net precipitation, and redistribution by wind forcing and mixing. The central Canada Basin is the freshest region of the Arctic Ocean, and the saltiest upper ocean is observed at the boundaries of the Eurasian Basin and the Barents Sea (Fig. 5.16, which illustrates salinity at a depth of 20 m, within the well-mixed surface layer for most of the year). Relative to the 1970s, the major upper-ocean salinity differences in 2013 (similar to 2012; see Timmermans et al. 2013a, figure 24) were saltier waters in the central Eurasian Basin and fresher waters in the Beaufort Gyre region of the Canada Basin. The main differences in upper-ocean salinity in 2013 relative to 2012 included saltier surface waters in the region north of Greenland and Ellesmere Island, Canada, and in the northern part of the East Siberian Sea/western Canada Basin.

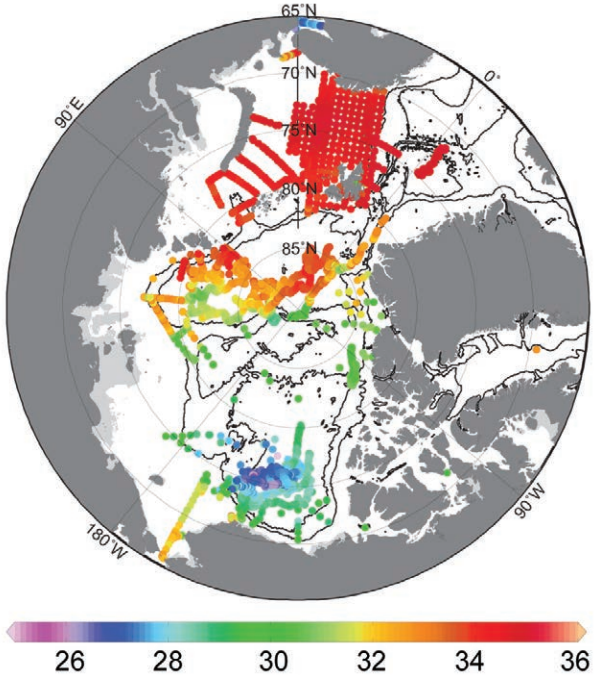

Fig. 5.16. Average salinity at 20-m depth in 2013. Contour lines show the 500-m and 2500-m isobaths. Salinities are reported using the Practical Salinity Scale (unitless). Data are from multiple sources, including various hydrographic expeditions by different countries and institutions, and ice-tethered profilers (http://www.whoi.edu/itp).

3) Freshwater content

Freshwater content in the Arctic Ocean has an important relationship to sea ice and climate; increased freshwater, for example, strengthens ocean stratification, impeding vertical heat transport from deeper waters. Liquid freshwater content in the upper Arctic Ocean basins showed an increasing trend from 1992 to 2012 of about 600 ±300 km^3 yr^{-1}, based on observed salinity profiles (Rabe et al. 2014). The maximum liquid freshwater content anomaly is centered in the Beaufort Gyre (Fig. 5.17). In total, during 2003–13 the Beaufort Gyre accumulated more than 5000 km^3 of freshwater (measured relative to a salinity of 34.8), a gain of approximately 25% (update to Proshutinsky et al. 2009) compared to the 1970s (see figure 5.24b in Timmermans et al. 2013b). Most of this increase occurred between 2004 and 2008.

In 2013, a reduction in freshwater content by about 7% was observed relative to 2012 (*cf.* Timmermans et al. 2013b, figure 5.24c). This reduction may be attributed in part to stronger cyclonic (counterclockwise) wind forcing in summer 2013 (compared to previous years) that drove divergence of surface waters in the region. It is of note that trends in Beaufort Gyre heat

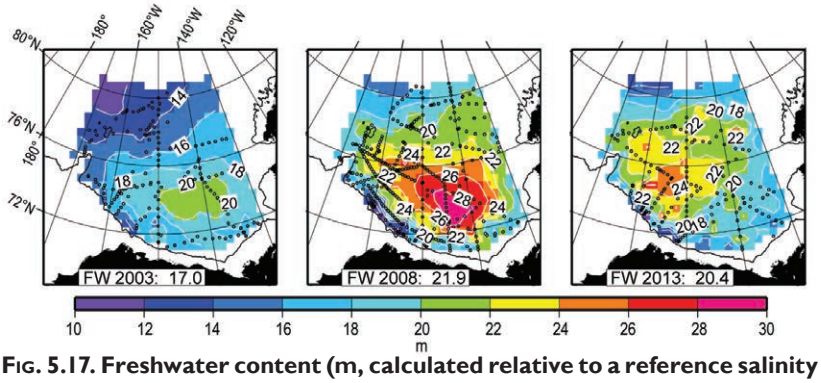

Fig. 5.17. Freshwater content (m, calculated relative to a reference salinity of 34.8) in the Beaufort Gyre of the Canada Basin based on hydrographic surveys in 2003, 2008, and 2013. Inset numbers at the bottom of each panel give total freshwater volume (×1000 km^3) in the region. Black dots depict hydrographic station locations. Data are from the Beaufort Gyre Observing System (BGOS)/Joint Ocean Ice Studies (JOIS) project (http://www.whoi.edu/beaufortgyre) and other Canada Basin expeditions.